



## King's Research Portal

DOI:

[10.1007/978-3-030-58104-6\\_20](https://doi.org/10.1007/978-3-030-58104-6_20)

[Link to publication record in King's Research Portal](#)

*Citation for published version (APA):*

Hans Natalius, & Tiwari, M. K. (2021). Design, Static and Performance Analysis of a Parallel Robot for Head Stabilisation in Vitreoretinal Surgery. In *Mechanisms and Machine Science* (Vol. 93, pp. 169-179). (Mechanisms and Machine Science; Vol. 93). [https://doi.org/10.1007/978-3-030-58104-6\\_20](https://doi.org/10.1007/978-3-030-58104-6_20)

### **Citing this paper**

Please note that where the full-text provided on King's Research Portal is the Author Accepted Manuscript or Post-Print version this may differ from the final Published version. If citing, it is advised that you check and use the publisher's definitive version for pagination, volume/issue, and date of publication details. And where the final published version is provided on the Research Portal, if citing you are again advised to check the publisher's website for any subsequent corrections.

### **General rights**

Copyright and moral rights for the publications made accessible in the Research Portal are retained by the authors and/or other copyright owners and it is a condition of accessing publications that users recognize and abide by the legal requirements associated with these rights.



- Users may download and print one copy of any publication from the Research Portal for the purpose of private study or research.
- You may not further distribute the material or use it for any profit-making activity or commercial gain
- You may freely distribute the URL identifying the publication in the Research Portal

### **Take down policy**

If you believe that this document breaches copyright please contact [librarypure@kcl.ac.uk](mailto:librarypure@kcl.ac.uk) providing details, and we will remove access to the work immediately and investigate your claim.



# Design, Static and Performance Analysis of a Parallel Robot for Head Stabilisation in Vitreoretinal Surgery

Hans Natalius<sup>1</sup>✉, Patrice Lambert<sup>2</sup>, Manish K. Tiwari<sup>1</sup> ,  
Lyndon da Cruz<sup>1,3</sup>, and Christos Bergeles<sup>2</sup> 

<sup>1</sup> University College London, Gower St, London WC1E 6BT, UK  
[nataliushans@gmail.com](mailto:nataliushans@gmail.com)

<sup>2</sup> King's College London, Strand, London WC2R 2LS, UK

<sup>3</sup> Moorfields Eye Hospital, 162 City Rd, London EC1V 2PD, UK

**Abstract.** This paper explores the requirements-based design and static analysis of a 6 Degree-of-Freedom parallel robotic headrest, of novel architecture, to counter head motion in vitreoretinal surgery. Upcoming therapy delivery interventions require micro-precision but should ideally take place under local anaesthesia. Therefore, breathing, spasmodic motions, and even snoring that often occurs need to be accounted for and if possible counteracted. Passive approaches that aim to constrain the patient's head have not yet been fruitful, while invasive stereotactic fixation is naturally not an option. The proposed design respects ergonomic and surgical constraints to act as a headrest that will ultimately counteract patient motion. Static models are developed to understand the architecture's characteristics, and performance metrics are devised for design evaluation. Finally, a prototype is presented.

**Keywords:** Parallel robot · Surgical robot · Kinematics

## 1 Introduction

Stem cell implantation and gene vector delivery are envisioned as sight-restoring vitreoretinal surgical interventions [1, 2]. To maximise the efficacy of therapeutics, injection precision of  $10\ \mu\text{m}$  is required. The surgeon's physiological hand tremor and patient's head movement, however, are proving a challenge in achieving the required positioning accuracy. Physiological hand tremor is on the order of  $200\ \mu\text{m}$  [3], while patient head motion can be as much as  $11\ \text{mm}$  [4]. While many solutions to mitigate hand tremor are being researched [5], methods to reduce the patient's head movement have been less explored. Head movements that occur such as when a patient snores, breathes, or sneezes, raise the risk of complications. Therefore, a method to stabilize the patient's head during ophthalmic surgery needs to be devised.

Examined approaches that aim to mitigate head movement have so far focused on trying to restrain the head. Examples include the head fixation device for iRAM!S robot [6] and the Granular-Jamming Headband [7]. Our article explores the possibility of a robotic headrest that can actively counter the patient’s head movements. As the headrest needs to perform motions whilst supporting the weight of the head, a parallel robot was chosen as the base system. Parallel manipulators combine high rigidity and low inertia, resulting in a faster dynamical response than serial manipulators. They also present higher accuracy due to their rigidity against unwanted movement. Although currently there are many available parallel robotic systems with 6 Degrees of Freedom (DoF) on the market, for example the Physik Instrumente H-825 6-Axis hexapod [8] and the HexGen HEX300-230HL Hexapod [9], design constraints and operational requirements arising in ophthalmic surgery render the existing manipulators unsuitable as active headrests. Therefore, a robotic headrest with a new parallel kinematic architecture alongside performance evaluation metrics related to our application’s requirements were developed.

## 2 Methods

This section presents the manipulator design approach, its static model, and analysis of its workspace and performance against clinical requirements.

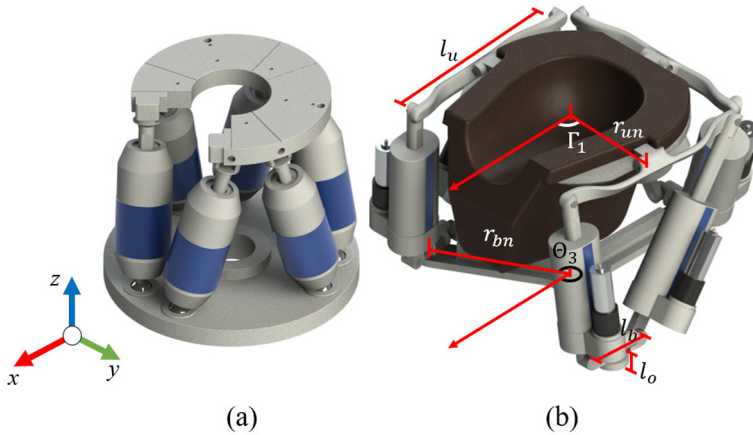


**Fig. 1.** Possible locations of the neck space in: (a) traditional Hexapod with a section between two actuators removed, and (b) the proposed manipulator.

**Manipulator Requirements:** For acceptance in a vitreoretinal surgical setting, the proposed manipulator needs to mitigate patient’s head movement whilst preserving the ergonomics for the surgeons and retaining patient comfort. To design a manipulator that can fulfill these functions, a set of requirements is defined.

To stabilize a lying patient’s head, the manipulator needs to apply a counter-motion with the same magnitude. A recent study showed that during surgery the patient’s head drifts for up to 11 mm along the horizontal plane ( $XY$ ). However, patient’s head drift along the global vertical direction ( $Z$ ) and rotation along an arbitrary axis needs to be anticipated as well [4]. Since the head moves and rotates in 3D space, the proposed manipulator architecture needs to possess 6-DoF, to reach any position within its workspace under any orientation. The workspace needs to be at least as big as the magnitude of the head drift, while also adjustable to adapt to different patient’s head position.

**Table 1.** Manipulator target specification

Requirement	Value
Resolution	10 $\mu\text{m}$
Translational Workspace diameter and height	88 mm, 61 mm
Rotational Workspace $\theta_x, \theta_y, \theta_z$	$\pm 5^\circ, \pm 5^\circ, \pm 5^\circ$
DoF	6
Load capacity	30 kg
Maximum height at Workspace Bottom Point	300 mm

As a safety measure in head stabilization, a cylindrical-shaped workspace that fits a  $50 \times 50 \times 50 \text{ mm}^3$  cube within it was chosen, with the addition of 11 mm on all directions to account for the magnitude of the head drift. To cover the required volume, the cylindrical-shaped workspace should have a minimum diameter of 88 mm, and vertical motion of 61 mm. Furthermore, while there is no identified value of a patient head’s rotation during surgery, we select a  $\pm 5^\circ$  rotation relative to all three global axes indicated in Fig. 1, as a requirement to accommodate extreme motions. The resolution target for the headset was selected to be the same as the  $10 \mu\text{m}$  resolution required for retinal therapy delivery.

In terms of load carrying, the manipulator must support the weight of the head, the headrest pillow, and all attached components in a dynamic setting. The human head on average weights 4.3–5.3 kg [10], while the headrest pillow (including metal supports) is approximated at 4–6 kg. The weight of the manipulator components to be carried is estimated at a maximum 3.5 kg. Therefore, the rounded up weight that the manipulator needs to carry is considered 15 kg. Considering a safety factor of at least 2 to account for purposeful/forceful motions for head-posture adaptation, we arrive at a requirement of 30 kg as the manipulator’s load-bearing capacity under motion. Finally, the manipulator must preserve the ergonomics for the surgeon and retain patient comfort. This can be achieved by embedding the headrest within the manipulator. As the height of existing headrests are on the order of 180 mm (measured in the clinic), the maximum height of the proposed manipulator when the upper platform is at its lowest operational position, which is referred as the workspace bottom point, should be maximum 300 mm. The requirements for the proposed manipulator are summarised in Table 1.

**Manipulator Design Architecture:** As is common in 6-DoF parallel robots, the general design of the manipulator architecture comprises a lower platform that functions as a base, an upper platform that acts as the end-effector of the system, and 6 linear actuators connecting the two. The headrest pillow will be mounted within the perimeter of the upper platform, as shown in Fig. 1b, so that the height of the manipulator respects the requirements listed in Table 1. The advantage of this configuration is that the center of mass of the head will be close to the upper platform centre-point, which increases the mechanical stability of the system. However, as the patient's head will rest deeper within the upper platform perimeter, dedicated space is required to accommodate their neck. One way to achieve this is by making space between two of the manipulator's actuator attachment points on the upper platform.

In traditional hexapods, cutting the upper platform between the two actuator attachment points as shown in Fig. 1(a) will not provide enough space to accommodate the patient's neck due to the interference caused by the axis-symmetric arrangement of the actuators. To maintain and enhance manipulator mechanical stability while enabling the platform to accommodate lower pillow position, we designed a parallel architecture where the 6 actuators are grouped into 3 Leg-Pairs. Each Leg-Pair always forms an imaginary local plane (Leg-Plane), perpendicular to its normal vector  $\hat{\mathbf{n}}$  regardless of the position and orientation of the upper platform.

The manipulator upper platform is connected by three 1-DoF rotary joints to three upper links, with their rotation axis located on the local  $XY$  plane of the upper platform at point  $U_0$  and oriented along the vector  $\hat{\mathbf{s}}_1$ , perpendicular to the vector  $\mathbf{c}$ , as shown in Fig. 2. Each upper link, together with two prismatic linear actuators and a lower link form a single Leg-Pair. The upper link is connected on both ends to the two actuators by 1-DoF rotary joints located at  $U_1$  and  $U_2$ , whereas the two actuators are also connected to the lower links by 1-DoF rotary joints, located at  $B_1$  and  $B_2$ . The rotation axes of these 4 1-DoF rotary joints are parallel to the normal  $\hat{\mathbf{n}}$  of the Leg-Plane. The two prismatic linear actuators are located between points  $U_1$  and  $B_1$ , and  $U_2$  and  $B_2$ , respectively. Finally, each lower link is connected to the lower platform by a 2-DoF universal joint located at point  $B_0$ , with 1 joint oriented on the Leg-Plane along  $\hat{\mathbf{s}}_2$  and 1 joint parallel to the the global  $Z$  Axis along  $\hat{\mathbf{s}}_3$ . The four-bar linkage actuator unit possess 3-DOF, which combined with the 3 1-DOF rotary joint, provide the manipulator upper platform the capability to move to any position and orientation within the workspace. By combining the linear actuators two-by-two in each leg-pairs, the proposed arrangement can provide space for the patient's neck by increasing the separation angle between two of its leg-pairs.

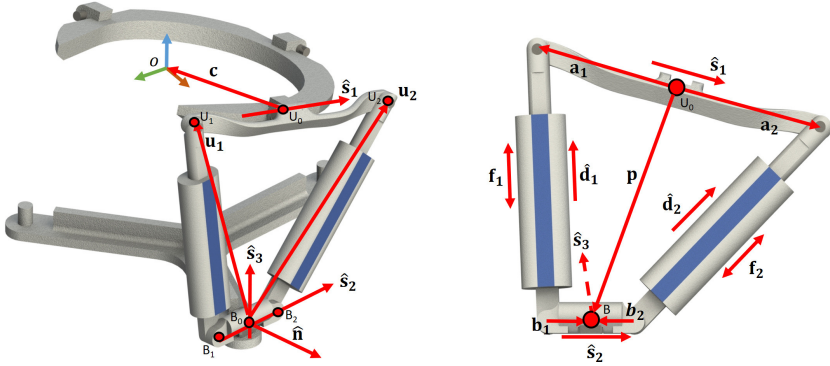


**Fig. 2.** The proposed manipulator architecture: The notation used in the kinematic model. The 3 identical Leg-Pairs can be modelled the same way.

**Inverse Position Kinematics:** Inverse position kinematics are briefly introduced in support of the expanded statics derivation in the subsequent section. Figure 2 shows the notation used to establish the relation between the position and orientation of the end-effector  $\mathbf{v} = [x \ y \ z \ \theta_x \ \theta_y \ \theta_z]^T$  and all the kinematic elements of the design, including the length of the prismatic actuators. For each leg, position of joints  $U_1$  and  $U_2$  are invariant to the upper platform local frame  $O$ , while the base point  $B_0$  is invariant in the base frame. The orientations of the joint axis vectors  $\hat{\mathbf{s}}_1$  and  $\hat{\mathbf{s}}_3$  are also invariant in their respective frames. The only unknown is therefore the orientation of  $\hat{\mathbf{s}}_2$ . This vector is perpendicular to both  $\hat{\mathbf{s}}_3$  and  $\mathbf{n} = \mathbf{u}_1 \times \mathbf{u}_2$ , *i.e.* the normal to the plane of the leg. Once  $\hat{\mathbf{s}}_2 = \hat{\mathbf{s}}_3 \times \hat{\mathbf{n}}$  is known for each leg, the configuration of the device can be fully established.

**Static Model and Jacobian Matrix:** This section presents the analytical model for the force transmission from the 6 actuators to the end-effector. The derived model was cross-validated with numerical derivatives of the inverse kinematics model.

To achieve static equilibrium in a given configuration, the sum of forces and moments on all rigid bodies must be zero. As it is the case for any parallel structure, the total forces and moments acting on the top platform are a linear combination of the sum of the forces and moments on each leg. The static analysis can therefore be calculated initially for each leg independently by the leg Jacobian matrix  $J_l$ . We will use the notation of Fig. 2 for a single leg-pair and retrieve the linear relation

$$\begin{bmatrix} \mathbf{f}_e(3 \times 1) \\ \boldsymbol{\tau}_e(3 \times 1) \end{bmatrix} = J_{l(6 \times 2)} \begin{bmatrix} f_1 \\ f_2 \end{bmatrix}, \tag{1}$$

where  $f_1$  and  $f_2$  are the forces produced by the two actuators of the leg and  $\mathbf{f}_e$  and  $\boldsymbol{\tau}_e$  are the forces and moments at the attachment point  $Uo_n$  (top link, middle).

The total forces and moments can be broken down into a component that lies in the plane of the leg, and a component that is normal to that plane such that  $\mathbf{f}_e = \mathbf{f}_{e,p} + \mathbf{f}_{e,n}$  and  $\boldsymbol{\tau}_e = \boldsymbol{\tau}_{e,p} + \boldsymbol{\tau}_{e,n}$ . Note that the vectors in this section can be computed in any reference frame as long as the same frame is used for all vectors.

On one hand, the calculation of the reaction forces in the plane ( $\mathbf{f}_{e,p}$ ), and the moments normal to the plane ( $\boldsymbol{\tau}_{e,n}$ ) are straightforward. In matrix form, we have

$$\begin{bmatrix} \mathbf{f}_{e,p} \\ \boldsymbol{\tau}_{e,n} \end{bmatrix} = \begin{bmatrix} \hat{\mathbf{d}}_1 & \hat{\mathbf{d}}_2 \\ \hat{\mathbf{d}}_1 \times \mathbf{a}_1 & \hat{\mathbf{d}}_2 \times \mathbf{a}_2 \end{bmatrix} = \begin{bmatrix} f_1 \\ f_2 \end{bmatrix} \quad (2)$$

On the other hand, the force normal to the plane  $\mathbf{f}_{e,n}$  and the moments in the plane  $\boldsymbol{\tau}_{e,n}$  require more elaborate calculations. Conceptually, these forces and moments are created because the universal joint at base point  $Bo_n$  cannot constrain the moment normal to the plane without creating additional moments in that plane.

Indeed, the moment applied on the base platform by the actuators is given by  $\boldsymbol{\tau}_{b,n} = f_1(-\hat{\mathbf{d}}_1 \times \mathbf{b}_1) + f_2(-\hat{\mathbf{d}}_1 \times \mathbf{b}_1)$ , which is always directed along  $\hat{\mathbf{n}}$ , *i.e.* normal to the plane. However, the only reaction moment allowed by the universal joint on the base is along the direction perpendicular to both of its joints, *i.e.* along  $\hat{\mathbf{s}}_3 \times \hat{\mathbf{s}}_2$ . Therefore, the total reaction moment on the base  $\boldsymbol{\tau}_b = \boldsymbol{\tau}_b(\hat{\mathbf{s}}_3 \times \hat{\mathbf{s}}_2)$  is such that its vector projection onto  $\hat{\mathbf{n}}$  is equal to  $\boldsymbol{\tau}_{b,n}$ .

While the  $\boldsymbol{\tau}_{b,n}$  component of  $\boldsymbol{\tau}_b$  reaches static equilibrium due to the forces  $f_1$  and  $f_2$  created by the actuators, the residual moment  $\boldsymbol{\tau}_{b,p} = \boldsymbol{\tau}_b - \boldsymbol{\tau}_{b,n} = \boldsymbol{\tau}_{b,p}(\hat{\mathbf{n}} \times \hat{\mathbf{s}}_2)$  lies in the Leg-Pair plane and must be compensated by forces and moments applied at the leg attachment point  $Uo_n$ . In matrix form:

$$[-\hat{\mathbf{s}}_3 \times \hat{\mathbf{s}}_2 \quad \hat{\mathbf{n}} \times \hat{\mathbf{s}}_2] \begin{bmatrix} \boldsymbol{\tau}_b \\ \boldsymbol{\tau}_{b,p} \end{bmatrix} = [\hat{\mathbf{d}}_1 \times \mathbf{b}_1 \quad \hat{\mathbf{d}}_2 \times \mathbf{b}_2] \begin{bmatrix} f_1 \\ f_2 \end{bmatrix} \quad (3)$$

For given forces  $f_1$  and  $f_2$ , this constitutes a system of three equations and two unknowns. A Moore-Penrose pseudoinverse (+) can be used to find a least-squares solution to a system of linear equations that lacks a unique solution. However, since all vectors in this system lie in the same plane normal to  $\hat{\mathbf{s}}_2$ , only 2 out of the 3 equations are independent. Thus, the use of the pseudoinverse produces the exact system solution, and the residual moment  $\boldsymbol{\tau}_{b,p}$  is

$$\boldsymbol{\tau}_{b,p} = [\mathbf{0}_{3 \times 1} \quad \hat{\mathbf{n}} \times \hat{\mathbf{s}}_2] [-\hat{\mathbf{s}}_3 \times \hat{\mathbf{s}}_2 \quad \hat{\mathbf{n}} \times \hat{\mathbf{s}}_2]^+ [\hat{\mathbf{d}}_1 \times \mathbf{b}_1 \quad \hat{\mathbf{d}}_2 \times \mathbf{b}_1] \begin{bmatrix} f_1 \\ f_2 \end{bmatrix} \quad (4)$$

To keep notation compact, (4) will be denoted as  $\boldsymbol{\tau}_{b,p} = J_1 [f_1 \quad f_2]^T$ , where index 1 in  $J_1$  simply refers to the first building block of the complete Jacobian matrix  $J$ .

The residual moment  $\boldsymbol{\tau}_{b,p}$  at the base of the leg lies in the plane of the Leg-Pair and must be compensated by forces and moments applied at the leg attachment point  $Uo_n$ . The two ways of creating moments in that plane are by a linear force  $\mathbf{f}_{e,n}$  perpendicular to the plane, and a moment  $\boldsymbol{\tau}_{e,p}$  in the plane itself, which are respectively orthogonal to vectors  $\mathbf{f}_{e,p}$  and  $\boldsymbol{\tau}_{e,n}$  described in (2).

Because of the revolute joint with axis  $\hat{\mathbf{s}}_1$  located at  $Uo_n$ , the direction of  $\boldsymbol{\tau}_{e,p}$  at this point must be aligned with  $\hat{\mathbf{n}} \times \hat{\mathbf{s}}_1$  while a force  $f_{e,n}$  at this point will create a moment  $f_{e,n}(\hat{\mathbf{n}} \times \mathbf{p})$ , with  $p$  being a vector from  $Uo_n$  to  $Bo_n$ . In static equilibrium:

$$[\hat{\mathbf{n}} \times \mathbf{p} \ \hat{\mathbf{n}} \times \hat{\mathbf{s}}_1] \begin{bmatrix} f_{e,n} \\ \boldsymbol{\tau}_{e,p} \end{bmatrix} = -J_1 \begin{bmatrix} f_1 \\ f_2 \end{bmatrix} \quad (5)$$

Since all the vectors lie in the same plane, only 2 of the 3 equations are independent. The pseudoinverse can be used for the exact solution for  $\mathbf{f}_{e,n}$  and  $\boldsymbol{\tau}_{e,p}$ :

$$\begin{bmatrix} \mathbf{f}_{e,n} \\ \boldsymbol{\tau}_{e,p} \end{bmatrix} = - \begin{bmatrix} \hat{\mathbf{n}} & \mathbf{0}_{3 \times 1} \\ \mathbf{0}_{3 \times 1} & \hat{\mathbf{n}} \times \hat{\mathbf{s}}_1 \end{bmatrix} [\hat{\mathbf{n}} \times \mathbf{p} \ \hat{\mathbf{n}} \times \hat{\mathbf{s}}_1]^+ J_1 \begin{bmatrix} f_1 \\ f_2 \end{bmatrix} \quad (6)$$

Adding (6) and (2) gives us the linear relation between the actuator forces  $f_1$  and  $f_2$  and the total reaction forces and moments  $\mathbf{f}_e$  and  $\boldsymbol{\tau}_e$  described in (1). The latter, however, only describes the forces for one leg at its attachment point.

We are interested in the effect of all three legs at the point  $O$  located in the middle of the end-effector platform. The force of leg  $i$  at point  $O$  is given by

$$\begin{bmatrix} \mathbf{f}_i \\ \boldsymbol{\tau}_i \end{bmatrix} = \begin{bmatrix} I_{(3 \times 3)} & \mathbf{0}_{(3 \times 3)} \\ [\mathbf{c}_i]_{\times} & I_{(3 \times 3)} \end{bmatrix} J_i \begin{bmatrix} f_{1i} \\ f_{2i} \end{bmatrix} = J_{li} \begin{bmatrix} f_{1i} \\ f_{2i} \end{bmatrix} \quad (7)$$

where  $[\mathbf{c}_i]_{\times}$  is the cross-product matrix of vector  $\mathbf{c}_i$  going from leg attachment point  $Uo_i$  to end-effector point  $O$ . Now, we can assemble all three legs as:

$$\begin{bmatrix} \mathbf{f} \\ \boldsymbol{\tau} \end{bmatrix} = \begin{bmatrix} J_{l1} \\ J_{l2} \\ J_{l3} \end{bmatrix} [f_{11} \ f_{21} \ f_{12} \ f_{22} \ f_{13} \ f_{23}]^T = \mathbf{J}\mathbf{F} \quad (8)$$

Due to the power conservation principle,  $J$  can be used to establish the inverse velocity kinematics as  $\mathbf{q} = J^T \mathbf{v}$  where  $\mathbf{q}$  is the length of the 6 actuators. Another way to obtain  $J^T$  is by numerical derivation of the inverse position kinematics. Numerical evaluations of  $J^T$  was performed all over the workspace, converging to the same value for the Jacobian matrix  $J$  obtained analytically in this section.

**Metrics for Performance Analysis:** We consider the reachable workspace, end-effector resolution for unit actuation stroke inputs (resolution ratio), and end-effector force output for unit actuation force input (force ratio). Stiffness and dynamics were not evaluated, and are left for future work.

It is well known that parallel manipulators are prone to parallel singularities inside their workspace where  $J^T \mathbf{v}_p = \mathbf{0}$  and control in a particular direction  $\mathbf{v}_p$  is lost. As manipulator workspace, we define the volume in which the upper platform can move and rotate without encountering any singularity. It was analyzed



by sampling the determinant and the condition number of the manipulator Jacobian matrix  $J$  within a range of positions and orientations that cover the desired workspace. To numerically identify singularities given the sampling intervals, we detected sign changes of the Jacobian determinant. The final robot workspace should not exhibit singularities.

The second performance metric is the end-effector resolution given unit actuation inputs, see [11]. This method maps a 6D hyper-cube corresponding to the resolution in the actuator space to a zonotope corresponding to the resolution in the end-effector space, the farthest points of which in each dimension correspond to the end-effector resolution in that dimension. The final robot should exhibit a resolution ratio that, for appropriate actuators, should fulfill the requirements of Table 1.

Finally, the end-effector force ratio was evaluated within the entire workspace in the  $X$ ,  $Y$ , and  $Z$  direction, following the methodology presented in [12]. Using (8), the force ratio corresponds to the highest absolute element in  $\mathbf{F}$  needed among the 6 actuators to produce a unit force on the end-effector in one direction. This ratio will be used to determine the actuator force needed to meet the force requirements.

### 3 Results

The metrics described previously aid in understanding how a manipulator's performance varies as the design parameters change. We employed them in a design evaluation approach that will not be fully described in this submission. In the end, to accommodate the patient's neck,  $\Gamma_1$  was set at  $86^\circ$ , and subsequently  $\Gamma_2$ , and  $\Gamma_3$ , at  $180^\circ$ , and  $274^\circ$ , respectively. Furthermore, as the upper platform needs to be large enough to support both the head and the headrest,  $r_{u1}$ ,  $r_{u2}$  and  $r_{u3}$  were set at 140 mm. To prevent the three upper links colliding with each other,  $l_u$  was constrained to maximum 260 mm. The design parameters are shown in Table 2.

**Manipulator Workspace:** Workspace analysis of the final design resulted in a set of condition number maps, where each map describes the condition number of the manipulator Jacobian Matrix at sampling points on an X-Y plane, given an initial height and orientation for the manipulator. Condition number maps were evaluated for representative sets of heights and orientations to ensure the absence of singularities within the desired workspace. Figure 3a shows the inverted value of the condition number for each sampling point for the manipulator at  $Z = 280$  mm, which represents the bottom of the overall workspace and its most common starting configuration. As can be seen, no singularities are present. The condition number is fairly constant within the desired workspace (encircled), implying consistent manipulator behaviour. The design satisfies the requirements of Table 1.

**End-Effector Resolution:** End-effector resolution analysis performed on the proposed manipulator design resulted in six resolution ratio maps, where each map details the resolution of the upper platform in a translational or rotational axis relative to the resolution of the actuator sensor, which was represented as  $q_{max}$ , at each sampling point. In translational motion along the  $X$  axis direction, the resolution factor of the upper platform is observed to be between 1.14 and 1.91, with the

**Table 2.** Manipulator design parameter values

Design parameter	Value
$r_{un}$ : Length of imaginary line that connects upper platform center point to the rotary joint that connects the upper platform and the $n^{th}$ Leg-Pair upper link. Also referred as upper platform $n^{th}$ radius.	$r_{u1} = 140$ mm $r_{u2} = 140$ mm $r_{u3} = 140$ mm
$\Gamma_n$ : Angle of separation between the upper platform $n^{th}$ radius and the $x$ axis on the local $XY$ Plane.	$\Gamma_1 = 86^\circ$ $\Gamma_2 = 180^\circ$ $\Gamma_3 = 274^\circ$
$l_u$ : Upper link length.	$l_u = 260$ mm
$r_{bn}$ : Length of imaginary line that connects lower platform center point to the universal joint that connects the lower platform and the $n^{th}$ Leg-Pair lower link. Also referred as lower platform $n^{th}$ radius.	$r_{b1} = 175$ mm $r_{b2} = 180$ mm $r_{b3} = 175$ mm
$\Theta_n$ : Angle of separation between the lower platform $n^{th}$ radius and the $x$ axis on the global $XY$ Plane.	$\Theta_1 = 60^\circ$ $\Theta_2 = 180^\circ$ $\Theta_3 = 300^\circ$
$l_b$ : Lower link length.	$l_b = 76$ mm
$l_o$ : Vertical offset between the center of lower platform to the lower link axis of rotation.	$l_o = 40$ mm

average value of 1.66. The maximum and average resolution factor values remain similar to that of the  $X$  direction, with the maximum value of 1.89 for both the translational motion on the  $Y$  and  $Z$  axis, and average value of 1.68 and 1.66 for the translation motion on the  $Y$  and  $Z$  axis respectively. Finally, the resolution factor for rotational motion relative to the global axes is similar to that for translational motion.

**End-Effector Force:** The end-effector force ratio value for each sampling point within the manipulator theoretical workspace is shown as the manipulator end-effector force map, with three examples of the force map shown in Fig. 3b. Examination of the end-effector force ratio values within the desired workspace revealed the maximum end-effector force ratio value of 5.63 to 1, minimum value of 5.45 to 1, and average of 5.56 to 1. The minimum end-effector force ratio value will be used in determining the minimum actuator force that one actuator would need to exert.

**Manipulator Prototype:** A prototype was created based on the design parameters to evaluate the manipulator's performance in a manually actuated setting. The manipulator upper and lower platforms were made using acrylic plates, whereas complex components such as the joint were made using sintered nylon. Because the 1st iteration manipulator prototype will only be used for design evaluation, it is equipped with 6 non-motorized struts that represent the actuators. The manipulator prototype is shown in Fig. 4 alongside a Styrofoam head.

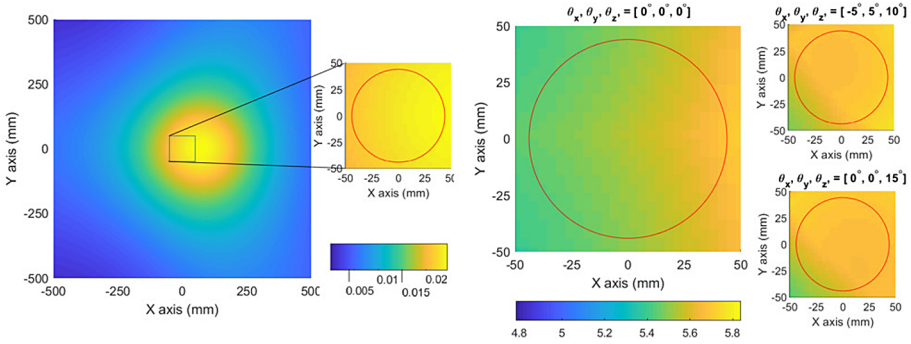


**Fig. 3.** Performance metric map for the proposed manipulator, **Left:** Sample condition number map with the workspace of interest marked within a circle, **Right:** End-effector force-ratio map for representative top platform orientations

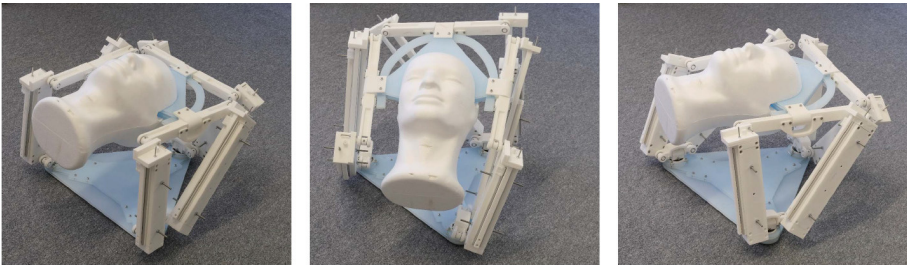


**Fig. 4.** The assembled prototype of the proposed manipulator. The large reachable workspace is illustrated, while the phantom head serves to indicate the accessibility of the manipulator’s interior.

### 4 Discussion and Conclusion

The designed manipulator needs to use sensors and actuators with a particular minimum specification in order to fulfill the operational requirements. The end-effector resolution analysis gave the maximum upper platform resolution factor value for translational motion of 1.91. Therefore, as the resolution factor value was rounded to 2, the manipulator needs to have linear actuator sensors with minimum resolution of at least  $5\ \mu\text{m}$  to fulfill the end-effector resolution target of  $10\ \mu\text{m}$ . Furthermore, because the manipulator needs to support a weight of 30 kg or 294 N, each actuator will need to be able to exert force of at least 54.04 N as the minimum value of the end-effector force ratio is 5.45 to 1. Therefore, the performance requirements are turned into actuation component requirements, and pave the road for motorisation.

**Acknowledgement.** This research was supported by the Sir Michael Uren Foundation. H. Natalius is supported by an Overseas Research Scholarship from University College London. H. Natalius, M. K. Tiwari and L. da Cruz are with University College London,

UK. Further, L. da Cruz is also with Moorfields Eye Hospital, London, UK. P. Lambert and C. Bergeles are with King's College London. H. Natalius and P. Lambert are equally contributing first authors, while C. Bergeles and L. Da Cruz are equally contributing senior authors. `hans.natalius.16@ucl.ac.uk`.

## References

1. Da Cruz, L., Fynes, K., Georgiadis, O., Kerby, J., Luo, Y.H., Ahmado, A., Vernon, A., Daniels, J.T., Nommiste, B., Hasan, S.M., Gooljar, S.B., Carr, A.J.F., Vugler, A., Ramsden, C.M., Bictash, M., Fenster, M., Steer, J., Harbinson, T., Willbrey, A., Tufail, A., Feng, G., Whitlock, M., Robson, A.G., Holder, G.E., Sagoo, M.S., Loudon, P.T., Whiting, P., Coffey, P.J.: Phase 1 clinical study of an embryonic stem cell-derived retinal pigment epithelium patch in age-related macular degeneration. *Nat. Biotechnol.* **36**, 1–10 (2018)
2. REP1 Gene Replacement Therapy for Choroideremia - Full Text View - ClinicalTrials.gov. <https://bit.ly/37MLG5N>. Accessed 02 Dec 2019
3. Riviere, C.N., Scott Rader, R., Thakor, N.V.: Adaptive canceling of physiological tremor for improved precision in microsurgery. *IEEE Trans. Biomed. Eng.* **45**, 839–845 (1998)
4. Brogan, K., Dawar, B., Lockington, D., Ramaesh, K.: Intraoperative head drift and eye movement: two under addressed challenges during cataract surgery. *Eye.* **32**, 1111–1116 (2018)
5. Vander Poorten, E., Riviere, C.N., Abbott, J.J., Bergeles, C., Nasser, M.A., Kang, J.U., Sznitman, R., Faridpooya, K., Iordachita, I.: Robotic retinal surgery. In: *Handbook of Robotic and Image-Guided Surgery* (2020)
6. Huang, K., Zhou, M., Lajblich, C., Lohmann, C.P., Knoll, A., Ling, Y., Lin, H., Nasser, M.A.: A flexible head fixation for ophthalmic microsurgery. In: *Proceedings - 2017 Chinese Automation Congress, CAC 2017*, pp. 6707–6710. Institute of Electrical and Electronics Engineers Inc. (2017)
7. Wirz, R., Lathrop, R.A., Godage, I.S., Burgner-Kahrs, J., Russell, P.T., Webster, R.J.: Can coffee improve image guidance? In: *Medical Imaging 2015: Image-Guided Procedures, Robotic Interventions, and Modeling*, p. 941513 (2015)
8. H-825 6-Axis Hexapod. <https://bit.ly/31by9Cc>. Accessed 02 Dec 2019
9. HexGen HEX300-230HL—Aerotech, Inc. <https://bit.ly/2u7CCd4>. Accessed 02 Dec 2019
10. Clauser, C., McConville, J., Young, J.: Weight, volume and center of mass of the human body. *Springf. NTIS.* (1969)
11. Cardou, P., Bouchard, S., Gosselin, C.: Kinematic-sensitivity indices for dimensionally nonhomogeneous jacobian matrices. *IEEE Trans. Robot.* **26**, 166–173 (2010)
12. Nokleby, S.B., Fisher, R., Podhorodeski, R.P., Firmani, F.: Force capabilities of redundantly-actuated parallel manipulators. *Mech. Mach. Theor.* **40**, 578–599 (2005)